Research papers

A fine spatial resolution estimation scheme for large-scale gross primary productivity (GPP) in mountain ecosystems by integrating an eco-hydrological model with the combination of linear and non-linear downscaling processes

Xinyao Xie [a,b], Ainong Li [a,b,*], Jie Tian [a,c], Changlin Wu [a,d], Huaan Jin [a]

[a] *Research Center for Digital Mountain and Remote Sensing Application, Institute of Mountain Hazards and Environment, Chinese Academy of Sciences, Chengdu 610041, China*
[b] *WangLang Mountain Remote Sensing Observation and Research Station of Sichuan Province, Mianyang 621000, China*
[c] *School of Civil Engineering and Geomatics, Southwest Petroleum University, Chengdu 610500, China*
[d] *College of Geological Engineering and Geomatics, Chang'an University, Xi'an 710054, China*

ARTICLE INFO

ABSTRACT

Accurate estimation of mountain vegetation gross primary productivity (GPP) at fine spatial resolutions offers opportunities to better understand mountain ecosystems' feedback to the global climate system. Eco-hydrological models have great advantages in simulating mountain vegetation photosynthesis, but their large-scale applications remain challenging at fine spatial resolutions due to the computing resources. In this work, a scheme by integrating an eco-hydrological model called Boreal Ecosystem Productivity Simulator-TerrainLab (BTL) with the linear and non-linear downscaling processes, was developed to obtain large-scale mountain vegetation GPP at the 30 m resolution over four watersheds. Firstly, two coarse spatial resolution GPP were simulated by BTL at 480 m and 120 m. Then, the 30 m resolution GPP was estimated by a linear downscaling process modelled at 120 m and a non-linear downscaling process modelled from 480 m to 120 m. The 30 m resolution BTL-simulated GPP was served as reference for evaluation. Results showed that the Root-Mean-Square-Error (*RMSE*) after downscaling was decreased by 110 $gCm^{-2}year^{-1}$ compared to the 120 m resolution BTL-simulated GPP (500 gCm^{-2} $year^{-1}$) at the 30 m resolution, highlighting the effectiveness of the proposed scheme in recovering the topographic variations of mountain vegetation GPP at fine spatial resolutions. Compared to the 120 m resolution BTL-simulated GPP (351 gCm^{-2} $year^{-1}$), RMSE after downscaling was decreased by 156 gCm^{-2} $year^{-1}$ at the 120 m resolution, indicating that the proposed scheme is feasible in correcting GPP errors at coarse spatial resolutions. More specifically, the non-linear downscaling process was observed to effectively improve GPP estimates after linear downscaling, suggesting that the spatial scaling errors in coarse estimates should be considered in the downscaling process. Our study indicates that the scheme that runs eco-hydrological models at coarse resolutions and then downscales them by surface heterogeneity is a practical approach for obtaining large-scale mountain vegetation GPP at fine spatial resolutions.

1. Introduction

Comprising approximately 24 % of the terrestrial surface (Kapos et al., 2000), mountain ecosystems provide a variety of essential services with farreaching effects on the climate system, such as carbon storage (Hilton and West, 2020), material resource provisioning (Bandyopadhyay et al., 1997), biodiversity conservation (Yang and Xu, 2003),

and water reservoirs (Viviroli et al., 2011). Over the last century, mountain vegetation has been regarded as an essential bio-indicator for monitoring the responses of terrestrial ecosystems to climate changes (Steinbauer et al., 2018). Accurate estimation of mountain vegetation gross primary productivity (GPP, defined as the total atmospheric carbon assimilated by vegetation) is crucial to understanding the functioning of mountain ecosystems and their feedback on the global climate

system (Chen et al., 2012; Xu et al., 2019; Yuan et al., 2019).

Currently, GPP can be mainly estimated by eddy covariance (EC) technology and remote sensing (RS)-based ecosystem models. The flux measurements of carbon, water, and energy are provided by various regional EC networks, such as the EUROPEFLUX (Aubinet et al., 2000), AsiaFlux (Mizoguchi et al., 2009), CarboAfrica (Henry et al., 2011), OzFlux (Beringer et al., 2016), and AMERIFLUX (Novick et al., 2018). These regional EC networks usually monitor the carbon exchange at the temporal resolution of half-hour (Bhattacharyya et al., 2013), but their spatial representation is always limited to several kilometers (Kljun et al., 2015). By combining the canopy-scale knowledge of photosynthesis and multi-scale vegetation information from RS observations (Xiao et al., 2019), ecosystem models make it feasible to estimate GPP at the large scale, which are mainly based on the approaches of machine learning (Jung, 2019; Tramontana et al., 2016), light use efficiency (LUE) (He et al., 2013; Running et al., 2004; Xiao et al., 2004), vegetation index (VI) (Sims et al., 2008; Wu et al., 2011), and process (Chen et al., 1999; Foley et al., 1996).

Over the past decades, ecosystem models for large-scale GPP estimation are always running at medium or coarse spatial resolutions, such as the Moderate-resolution Imaging Spectroradiometer (MODIS) GPP (Running et al., 2015), Vegetation Photosynthesis Model (VPM) GPP (Zhang et al., 2017), Light Response Function (LRF) GPP (Tagesson et al., 2021), and Global LAnd Surface Satellite (GLASS) GPP (Liang et al., 2021; Yuan et al., 2010). Such coarse or medium GPP datasets have been reported to have large uncertainties in mountain ecosystems because (1) the ignorance of surface heterogeneity within each coarse or medium modelling pixels would lead to obvious spatial scaling errors in the final estimates (Ahl et al., 2005; Ershadi et al., 2013; Xie et al., 2022) and (2) coarse or medium estimates would potentially lose the topographic characteristics of mountain vegetation GPP (Robinson et al., 2018; Wang et al., 2019b). Regarding the first spatial scaling issue, previous studies have made efforts to develop several spatial scaling algorithms by considering surface heterogeneity (Chen et al., 2013; Simic et al., 2004; Xie et al., 2021a), such as the vegetation type, vegetation density, and surface topography. Despite these spatial scaling algorithms could improve the coarse estimates of vegetation productivity, they still could not recover the topographic characteristics of mountain vegetation GPP, leaving the second issue unsolved.

Since several satellite sensors could offer fine spatial resolution vegetation information, fine spatial resolution vegetation GPP estimates can be obtained by directly running ecosystem models at fine spatial resolutions. For example, Robinson et al. (2018) executed the MODIS GPP algorithm at the 30 m resolution and created an improved dataset for the United States. Recently, Huang et al. (2022) also generated the global fine resolution of GLASS (Hi-GLASS) GPP dataset by running the two-leaf EC-LUE model at the 30 m resolution. By integrating fine spatial resolution RS-based information (e.g., Landsat VIs), current fine spatial resolution GPP datasets can further depict the effect of vegetation heterogeneity on photosynthesis, but neglect the surface topography in the carbon modeling process. Limited by the high computing resources, almost all the regional or global GPP datasets are generated from LUE-based or VI-based approaches, such as the aforementioned MODIS, GLASS, and VPM GPP (Huang et al., 2022; Robinson et al., 2018; Zhang et al., 2017). LUE-based or VI-based approaches always estimate GPP based on each single modeling pixel, while little attention has been paid to these ecological processes between pixels, i.e., soil water of higher-elevation pixels could move to lower-elevation pixels (Beven et al., 2021; Chen et al., 2005; Wigmosta et al., 1994).

In mountain ecosystems, surface topography has an apparent hydrological control on the water cycle (Beven et al., 2021; Chen et al., 2005; Wigmosta et al., 1994), and therefore the stomatal conductance (Harris et al., 2004; Jarvis, 1976; Tan et al., 2019), phenological dynamics (Band et al., 1993), and photosynthesis (Ju and Chen, 2005; Ju et al., 2006). It has been reported that surface topography is as important as vegetation heterogeneity in determining the spatial distributions

of vegetation productivity (Chen et al., 2013). For the above purposes, some eco-hydrological models have been developed to characterize the interaction between terrestrial carbon and water cycles in mountain ecosystems, such as the Boreal Ecosystem Productivity Simulator (BEPS)-TerrainLab (Govind et al., 2009) and Catchment Nutrients Management Model-DeNitrification-DeComposition Model (Zhang et al., 2018). Although such eco-hydrological models have great advantages in obtaining mountain vegetation GPP, their regional or global applications at fine spatial resolutions remain challenging due to the complicated model structures.

Rather than directly running eco-hydrological models at fine spatial resolutions, running eco-hydrological models at coarse spatial resolutions and then downscaling these estimates by surface heterogeneity, is a potential method to obtain fine spatial resolution mountain vegetation GPP at regional or global scales. Over the past decades, various algorithms have been proposed to downscale coarser resolution datasets to finer resolutions (Ma et al., 2017a; Ma et al., 2018; Ma et al., 2019b; Ma et al., 2017b). However, current spatial downscaling algorithms for carbon and water fluxes estimates usually assume that the relationship between coarse resolution estimates and surface heterogeneity is universal at fine spatial resolutions (Ke et al., 2017; Zhao et al., 2018), hereafter termed as the linear downscaling process. Such linear downscaling algorithms neglect the spatial scaling errors in coarse spatial resolution estimates, and therefore adopting these relationships obtained at coarse spatial resolutions to obtain fine spatial resolution estimates might have biases. To reduce the uncertainties caused by the spatial scaling errors in coarse spatial resolution estimates, it is necessary to improve the linear downscaling process by adding a process associated with the non-linear response of photosynthesis to environmental variations across spatial resolutions (hereafter termed the non-linear downscaling process).

Given the above insights, the main objectives of this study are to: (1) develop a fine spatial resolution estimation scheme for large-scale mountain vegetation GPP by integrating an eco-hydrological model with the combination of a linear downscaling process and a non-linear downscaling process, and (2) characterize the contributions of linear and non-linear downscaling processes in recovering the topographic characteristics of mountain vegetation GPP at fine spatial resolutions and correcting spatial scaling errors at coarse spatial resolutions. In this work, the proposed scheme was evaluated at four mountainous watersheds, and the outcomes can provide references for obtaining fine spatial resolution mountain vegetation GPP at regional or global scales.

2. Methodology

2.1. Description of the mountain vegetation GPP model

An eco-hydrological model (BEPS-TerrainLab V2.0, BTL) that considers the controls of surface topography on carbon and water cycles (Govind et al., 2009), was used to obtain mountain vegetation GPP in this work. In BTL, a flow mechanism is adopted to simulate the control of surface topography on the movement of groundwater between pixels. BTL also designs a four-leaf strategy to calculate the overstory canopy's photosynthesis (A_o), which can be briefly described as:

$$A_o = A_{sun} + A_{shd} \tag{1}$$

$$A_{sun} = A_{sun,unsat} \times LAI_{sun} \times u + A_{sun,sat} \times LAI_{sun} \times (1 - u) \tag{2}$$

$$A_{shd} = A_{shd,unsat} \times LAI_{shd} \times u + A_{shd,sat} \times LAI_{shd} \times (1 - u) \tag{3}$$

where $A_{sun,unsat}$ and $A_{sun,sat}$ are the net photosynthetic rates of the sunlit canopy with the states of unsaturated and saturated moisture, respectively; $A_{shd,unsat}$ and $A_{shd,sat}$ are the photosynthetic rates of the shaded canopy with the states of unsaturated and saturated moisture, respectively; LAI_{sun} and LAI_{shd} are the leaf area index (LAI) of sunlit canopy and

shaded canopy, respectively; u is the fraction of roots in the state of unsaturated moisture, and thus (1-u) represents the fraction of roots in the state of saturated moisture. The net photosynthetic rate of the four parts is calculated by a leaf-level model (Farquhar et al., 1980):

$$A = \min(W_c, W_j) - R_d \tag{4}$$

$$W_c = V_m \frac{C - \Gamma}{C + K_c(1 + O/K_o)} \tag{5}$$

$$W_j = J_m \frac{C - \Gamma}{4C + 8\Gamma} \tag{6}$$

where W_c and W_j are the gross photosynthetic rates limited by Rubiso and RuBP, respectively; R_d indicates the daytime leaf dark respiration; V_m and J_m are the maximum rates of carboxylation and electron transport, respectively; C and O are the concentrations of intercellular CO_2 and O_2, respectively; K_c and K_o are the Michaelis-Menten constants for CO_2 and O_2, respectively; Γ is the CO_2 compensation point without dark respiration. More descriptions of BEPS, Terrainlab, and BTL are provided in Chen et al. (1999), Chen et al. (2005), and Govind et al. (2009), respectively.

2.2. Downscaling-based scheme for obtaining fine spatial resolution mountain vegetation GPP

The proposed downscaling-based scheme for obtaining a 30 m resolution mountain vegetation GPP is shown in Fig. 1. According to the traditional downscaling method used in previous studies (Ke et al., 2017; Zhao et al., 2018), if assuming that the response of photosynthesis to environmental variations across spatial resolutions is linear, the relationship between GPP estimates and surface heterogeneity at coarse resolutions is feasible to estimate GPP at fine spatial resolutions (denoted as GPP_L). Considering the spatial scaling errors in coarse GPP estimates (Chen et al., 2013; Simic et al., 2004; Xie et al., 2021a), this study makes a step forward to correct the residual biases in GPP_L by modelling the non-linear response of mountain vegetation photosynthesis to environmental variations (denoted as GPP_{NL}). In this context, GPP at the 30 m spatial resolution (i.e., $GPP30\,L + NL$) is separated into a linear part (i.e., $GPP30\,L$) and a non-linear part (i.e., $GPP30\,NL$):

$$GPP^{30}_{L+NL} = GPP^{30}_L + GPP^{30}_{NL} \tag{7}$$

The detailed modelling processes of $GPP30\,L$ and $GPP30\,NL$ can be found in the following sections.

2.2.1. Modelling the linear downscaling process at the 120 m and 480 m resolutions

Firstly, GPP estimate at the spatial resolution of 120 m (i.e., $GPP120\,BTL$) and 480 m (i.e., $GPP480\,BTL$) is obtained by directly running the BTL model. Then, the relationships between BTL-simulated GPP and surface heterogeneity at 120 m (i.e., $f120\,L$) and 480 m (i.e., $f480\,L$) are modelled by the random forest algorithm:
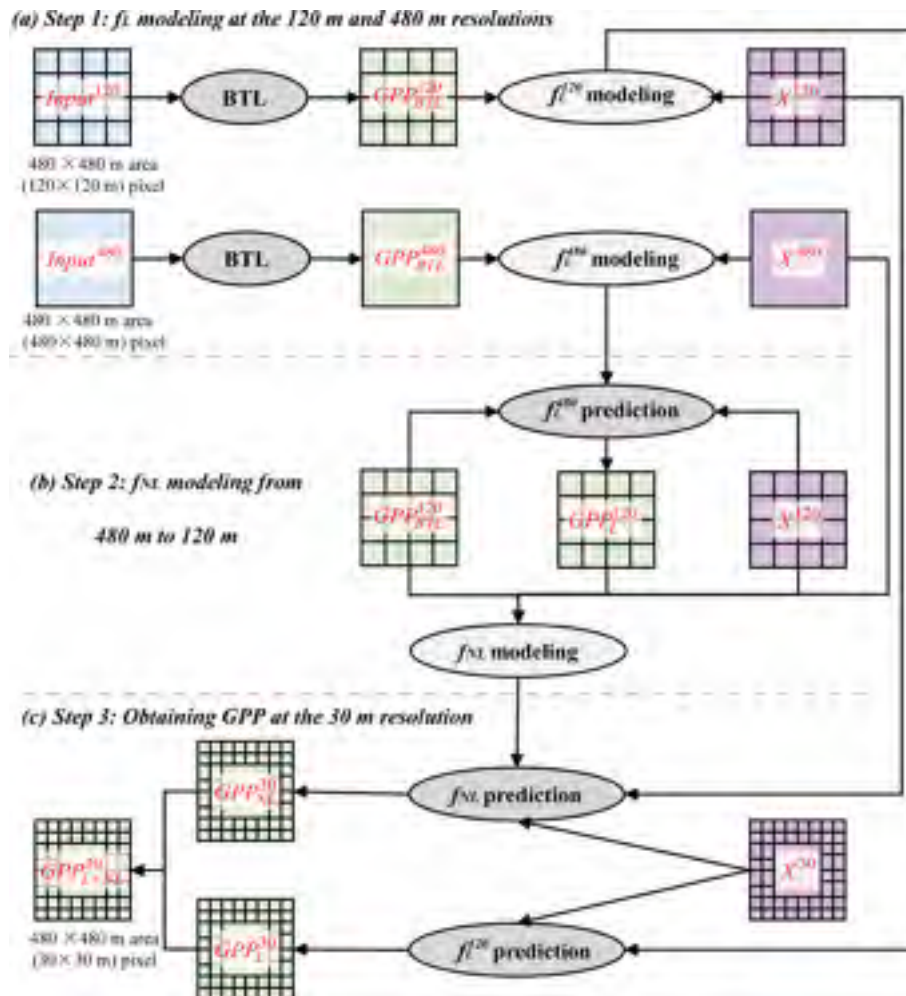

Fig. 1. Scheme for obtaining fine spatial resolution mountain vegetation GPP by integrating the BTL model with the combination of linear and non-linear downscaling processes.

$$GPP_{BTL}^{120} = f_L^{120}\left(X_{veg}^{120}, X_{top}^{120}, X_{met}\right) \tag{8}$$

$$GPP_{BTL}^{480} = f_L^{480}\left(X_{veg}^{480}, X_{top}^{480}, X_{met}\right) \tag{9}$$

where *X120 veg* and *X120 top* are the indicators for describing vegetation heterogeneity and surface topography at 120 m resolution, respectively; *X480 veg* and *X480 top* are the indicators for describing vegetation heterogeneity and surface topography at 480 m resolution, respectively; X_{met} represents the climatic indicators, including precipitation (*PRE*), radiation (*RAD*), and temperature (*TEM*) at the watershed scale. Based on previous studies (Chen et al., 2013; Xie et al., 2021a), this study expresses the vegetation heterogeneity by land cover (LC) and LAI, and describes the local and long-distance topographical variations by elevation, slope, aspect, topographic wetness index (TWI), and sky-view factor (SVF). The basis for selecting these factors can be found in Appendix S1. TWI and SVF can be calculated according to Sorensen et al. (2006) and Zaksek et al. (2011):

$$TWI = In\left(\frac{Facc}{\tan(S)}\right) \tag{10}$$

$$SVF = \frac{1}{n_d}\sum_{i=1}^{n_d}(1 - \sin(h_i)) \tag{11}$$

where *Facc* indicates the area of flow accumulation; *S* is the slope; h_i represents the angle of vertical altitude; n_d indicates the total number of directions.

Random forest is an ensemble-based algorithm by assuming that a set of predictors always perform better than an individual predictor (Breiman et al., 2001), which has been successfully and widely used in estimating biological parameters, such as GPP (Tramontana et al., 2016), LAI (Houborg and McCabe, 2018), soil moisture (Zhao et al., 2018), and land surface temperature (Zhao et al., 2019). During the regression process, a multitude of decision trees (the number was set as 500 in this work) are firstly constructed based on approximately-two-thirds of the training sample (i.e., bootstrap samples), and then are un-biasedly evaluated against the remaining one-third samples (i.e., 'out-of-bag' samples). The predicted values of all the individual trees in the "forest" are aggregated to obtain the final values.

2.2.2. Modelling the non-linear downscaling process from 480 m to 120 m resolution

In this step, the linear downscaling process modelled at 480 m resolution (i.e., *f480 L*) is firstly applied to obtain GPP at the 120 m resolution (i.e., *GPP120 L*):

$$GPP_L^{120} = f_L^{480}\left(X_{veg}^{120}, X_{top}^{120}, X_{met}\right) \tag{12}$$

where *X120 veg* and *X120 top* are the indicators for describing vegetation heterogeneity and surface topography at 120 m resolution, respectively; If the response of photosynthesis to environmental variations across spatial resolutions is linear, there should be no bias between *GPP120 BTL* and *GPP120 L*. However, there are inevitable residual biases due to the spatial scaling errors, and it can be calculated as:

$$GPP_{NL}^{120} = GPP_{BTL}^{120} - GPP_L^{120} \tag{13}$$

Finally, the relationship between *GPP120 NL* and the variations of surface heterogeneity from 120 m to 480 m (i.e., f_{NL}) is also modelled by the random forest algorithm:

$$GPP_{NL}^{120} = f_{NL}\left(X_{veg}^{120}, X_{top}^{120}, X_{veg}^{480}, X_{top}^{480}, X_{met}\right) \tag{14}$$

2.2.3. Obtaining GPP at the 30 m resolution by combining the linear and non-linear downscaling

According to the modelling processes associated with linear down-

scaling and non-linear downscaling, the modelled relationships are applied to the information of surface heterogeneity at the spatial resolutions of 30 m and 120 m:

$$GPP_L^{30} = f_L^{120}\left(X_{veg}^{30}, X_{top}^{30}, X_{met}\right) \tag{15}$$

$$GPP_{NL}^{30} = f_{NL}\left(X_{veg}^{30}, X_{top}^{30}, X_{veg}^{120}, X_{top}^{120}, X_{met}\right) \tag{16}$$

where *X30 veg* and *X30 top* are respectively the indicators for describing vegetation heterogeneity and surface topography at the spatial resolution of 30 m.

2.3. Experimental design

2.3.1. Study areas

As listed in Table 1, the proposed scheme was evaluated at four mountainous watersheds, namely CN-WL, JP-MBF, US-GLE, and CN-Cha. As shown in Fig. 2, the slope ranges of CN-WL, JP-MBF, US-GLE, and CN-Cha are 0-79°, 0-49°, 0-54°, and 0-27°, respectively. The the main vegetation types are needleleaf forest (NF), broadleaf forest (BF), mixed forest (MF), shrubland, grass, and crop.

2.3.2. Data source and processing

In this work, mainly-five datasets were used to drive the BTL model, which can be summarized as (1) the site-based daily meteorological data in the four watersheds, including incoming solar radiation, air temperature, and precipitation, (2) 30 m resolution LC maps acquired from Gong et al. (2013) and Xie et al. (2021b), (3) 30 m resolution and 8-day LAI maps generated from MODIS and Landsat datasets (Xie et al., 2021a; Xie et al., 2021b), (4) 30 m resolution elevation, slope, and aspect acquired from the Shuttle Radar Topography Mission Digital Elevation Model (SRTM DEM) (van Zyl, 2001), and (5) 250 m resolution soil type maps obtained from the Open Land Map (OLM) products (Hengl et al., 2017).

Besides the site-based meteorological data, all the other four datasets should be firstly prepared at the spatial resolution of 30 m. In the middle or coarse spatial resolution simulations of carbon and water fluxes over mountainous areas, previous studies always calculate slope and aspect at the fine spatial resolution and then aggregated them to coarser resolutions (Zhao et al., 2019). In this study, the soil type maps at the spatial resolution of 30 m were obtained from the coarse OLM maps by assuming the soil types of subpixels were same to those of the coarse pixels. Then, these 30 m resolution input datasets were aggregated to two coarse spatial resolutions following that (1) the LC and soil type of each 120 m or 480 m pixel were set as the major types of 30 m subpixels and (2) LAI, elevation, slope, and aspect were averaged to the 480 m or 120 m resolution.

Additionally, the available daily EC GPP estimates obtained from the global flux network (Arain and Restrepo-Coupe, 2005; Baldocchi et al., 2001; Guan et al., 2006; Matsumoto et al., 2008), were also adopted to evaluate the BTL model at the JP-MBF, US-GLE, and CN-Cha sites. Since CN-WL is a newly established station, the site-based measurements were insufficient to obtain reliable tower-based GPP (Wutzler et al., 2018). More descriptions of calculating tower-based GPP can be found at the website of https://www.bgc-jena.mpg.de.

2.3.3. Simulation procedure of BTL

In this work, the key biophysical parameter of BTL named maximum carboxylation rate across vegetation types was obtained from He et al. (2019), and other biophysical parameters were set following Liu et al. (2018). Besides these biophysical parameters, hydrological parameters of BTL were set according to the corresponding values in Govind et al. (2009). Previous studies associated with the spatial scaling of vegetation productivity were always conducted by annual values (Chen et al., 2013; Simic et al., 2004). In this work, all the GPP estimates from BTL were

Table 1
Descriptions of selected watersheds in this work.

Name	Latitude (°)	Longitude (°)	Areas (km^2)	Study year	Percentage of main vegetation types (%)					
					NF	BF	MF	Shrub	Grass	Crop
CN-Wl[a]	33.005	104.033	272.14	2020	28.55	1.54	12.98	7.24	27.49	0.00
JP-MBF[b]	44.387	142.319	151.14	2005	19.77	40.57	19.48	0.00	16.11	4.06
US-GLE[c]	41.367	−106.24	195.64	2010	76.95	0.70	0.07	0.01	21.79	0.07
CN-Cha[d]	42.403	128.096	114.26	2005	10.49	23.22	64.64	0.01	0.51	0.11

[a] Xie et al. (2021b).
[b] Matsumoto et al. (2008).
[c] Arain and Restrepo-Coupe (2005).
[d] Guan et al. (2006).
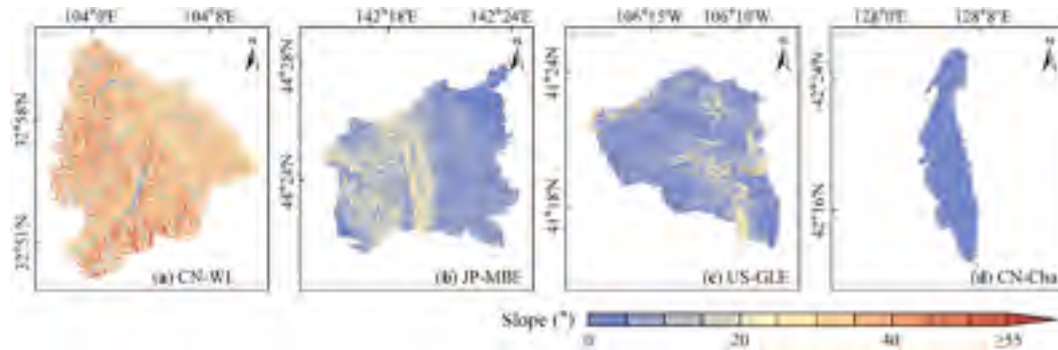
Fig. 2. Spatial distributions of slope over the (a) CN-WL, (b) JP-MBF, (c) US-GLE, and (d) CN-Cha watersheds.

simulated at a daily step, and then aggregated to annual values to perform the downscaling process.

2.3.4. Validation of the proposed scheme

EC technology could provide reliable carbon flux measurements, and thus EC GPP has been widely used to evaluate GPP estimates from various models over the past decades (Guan et al., 2021; Running et al., 2004; Zhang et al., 2017). To validate the proposed scheme, the GPP estimates obtained by running the BTL model at the 30 m resolution were served as the reference GPP (i.e., *GPP30 BTL*), and the reference GPP was firstly evaluated against daily EC GPP.

With regards to the effectiveness of the proposed downscaling-based scheme in recovering the topographic features of mountain vegetation GPP at the 30 m resolution, relationships between reference GPP and (1) 120 m resolution BTL-simulated GPP (resampled to 30 m resolution by assuming the values of subpixels were same to those of the coarse pixels), (2) GPP after linear downscaling, and (3) GPP after linear and non-linear downscaling were adopted as evaluation indicators. To further assess the advantage of the proposed scheme in correcting spatial scaling errors, relationships between aggregated reference GPP and (1) 120 m resolution BTL-simulated GPP (or aggregated to the 480 m resolution), (2) aggregated GPP after linear downscaling, and (3) aggregated GPP after linear and non-linear downscaling were also compared at 120 m and 480 m resolutions. In the above comparisons, the agreement index (*d*), Root-Mean-Square-Error (*RMSE*), and Mean-Absolute-Error (*MAE*) were selected as the indicators:

$$d = 1 - \frac{\sum_{j=1}^{N}\left(P_j - O_j\right)^2}{\sum_{j=1}^{N}\left(|P_j - \overline{O}| + |O_j - \overline{O}|\right)^2} \tag{17}$$

$$RMSE = \sqrt{\frac{1}{N}\sum_{j=1}^{N}\left(P_j - O_j\right)^2} \tag{18}$$

$$MAE = \frac{1}{N}\sum_{i=1}^{N}|P_j - O_j| \tag{19}$$

where *N* is the total number of 30 m, 120 m, or 480 m resolution pixels; O is the reference GPP at 30 m resolution, aggregated reference GPP at 120 m resolution, or aggregated reference GPP at 480 m resolution; P is the 120 m resolution BTL-simulated GPP, GPP after linear downscaling, and GPP after linear and non-linear downscaling prepared at 30 m, 120 m, and 480 m resolutions; $\overline{O}$ is the mean value of O.

## 3. Results and analysis

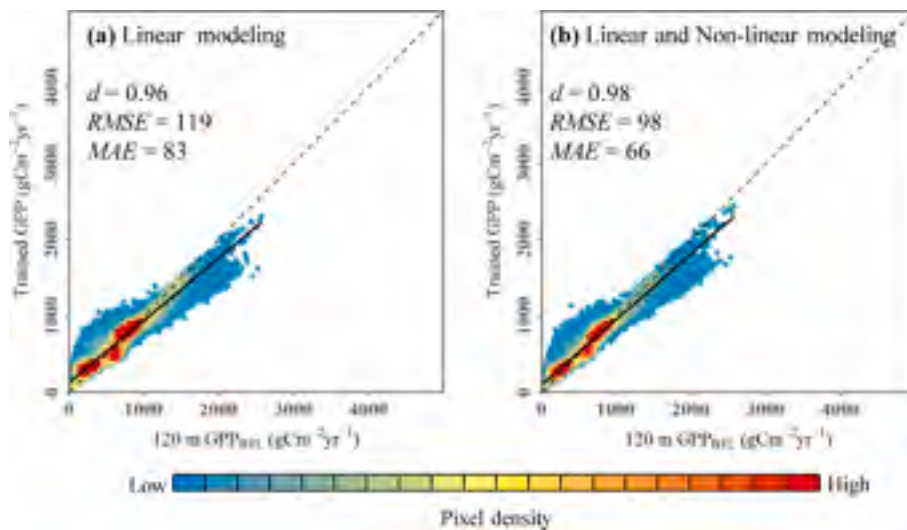### 3.1. Relationships between EC GPP and GPP estimates

Relationships between EC GPP and BTL-simulated GPP at the JP-MBF, US-GLE, and CN-Cha sites are presented in Fig. 3. Results showed that daily BTL-simulated GPP at the 30 m resolution had good relationships with EC GPP, characterized by *d* values of 0.83–0.96 and *RMSE* values of 0.59–2.76 gC m^{-2} day^{-1}. Compared to the BTL-simulated GPP estimates at the spatial resolution of 120 m, BTL-simulated GPP estimates at the spatial resolution of 30 m were observed to match better with EC GPP, with the *d* values increased by 0.02 to 0.12 and the *RMSE* values decreased by 0.04 to 0.87 gC m^{-2} day^{-1}.

3.2. Evaluation of the RF algorithm in modeling linear and non-linear relationships

Relationships between 120 m resolution BTL-simulated GPP and RF-trained GPP are presented in Fig. 4. Results showed that RF-trained GPP from the linear modeling process had a good relationship with the 120 m resolution BTL-simulated GPP, characterized by *d*, *RMSE*, and *MAE* values of 0.96, 119, and 83 gC m^{-2} yr^{-1}. As for the combination of linear and non-linear modeling processes, RF-trained GPP also matched well with the 120 m resolution BTL-simulated GPP, characterized by *d*, *RMSE*, and *MAE* values of 0.98, 98, and 66 gC m^{-2} yr^{-1}. Compared the linear modeling process, the combination of linear and non-linear modeling processes was observed to achieve a slight better performance, with *RMSE* and *MAE* values decreased by 21 and 17 gC m^{-2} yr^{-1}.
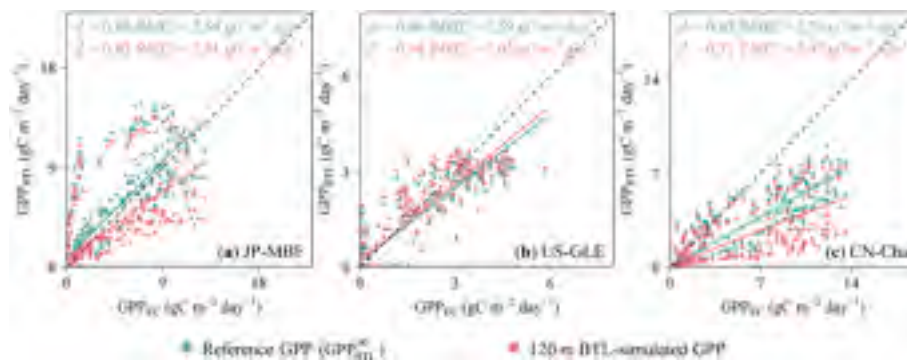
Fig. 3. Relationships between EC GPP (i.e., *GPP_EC*) and BTL-simulated GPP at (a) JP-MBF, (b) US-GLE, and (c) CN-Cha sites. Green and red represent the mean values of the central 1.5 km pixels in the daily BTL-simulated GPP at the spatial resolutions of 30 m (*GPP30 BTL*) and 120 m (*GPP120 BTL*), respectively. (For interpretation of the references to colour in this figure legend, the reader is referred to the web version of this article.)

Fig. 4. Relationships between 120 m resolution BTL-simulated GPP and RF-trained GPP. Subfigures (a) and (b) represent the linear modeling and the linear and non-linear modeling, respectively.

3.3. Comparisons of GPP estimates at the spatial resolution of 30 m

The spatial distributions of reference GPP and GPP after linear and non-linear downscaling at the 30 m resolution over the CN-WL watershed (Sub-Fig. 5 Aa-Ba) are presented as an example. As shown in Sub-Fig. 5Cb, 120 m resolution BTL-simulated GPP was observed to lose the most detailed characteristics over the whole watershed, and the major pixels with high values showed an obvious underestimation. After applying the linear and non-linear downscaling processes, the GPP estimates were observed to recover the major topographic features at the watershed scale, and the phenomenon of underestimation was alleviated.

The 30 m resolution relationships between reference GPP and 120 m resolution BTL-simulated GPP, GPP after linear downscaling, and GPP after both the linear and non-linear downscaling are illustrated in Sub-Fig. 6 Aa, Ba, and Ca. As for all the pixels over the four watersheds, the *d*, *RMSE*, and *MAE* values between reference GPP and 120 m resolution BTL-simulated GPP were 0.69, 500, and 341 gC m^{-2} year^{-1}, respectively. The *d*, *RMSE*, and *MAE* values were improved (1) by 0.07, 91, and 53 gC m^{-2} year^{-1} after the linear downscaling and (2) by 0.13, 110, and 63 gC m^{-2} year^{-1} after both the linear and non-linear downscaling, in comparisons with the 120 m resolution BTL-simulated GPP estimates.

The *d* values between reference GPP and 120 m resolution BTL-simulated GPP, after linear downscaling, and after both the linear and non-linear downscaling across vegetation types are listed in Table 2. At

the 30 m resolution, the *d* values of 120 m resolution BTL-simulated GPP in forest, shrub, grass, and crop pixels were 0.65, 0.70, 0.82, and 0.72, respectively. After applying the linear downscaling process, the *d* values of GPP estimates in forest, shrub, grass, and crop pixels were increased by 0.05, 0.13, 0.10, and 0.14, respectively. After applying both the linear and non-linear downscaling processes, the *d* values of GPP estimates in forest, shrub, grass, and crop pixels were increased by 0.12, 0.17, 0.12, and 0.17, respectively. Compared to the single linear downscaling, the combination of linear and non-linear downscaling processes increased the *d* values by 0.07, 0.04, 0.02, and 0.03 in forest, shrub, grass, and crop pixels.

3.4. Comparisons of GPP estimates at the spatial resolutions of 120 m and 480 m

The spatial characteristics of aggregated reference GPP, 120 m resolution BTL-simulated GPP (or aggregated to the 480 m resolution), aggregated GPP after linear downscaling, and aggregated GPP after linear and non-linear downscaling at the 120 m resolution (Sub-Fig. 5 Ab-Cb) and 480 m resolution (Sub-Fig. 5 Ac-Cc) over the CN-WL watershed are presented as an example. At the 120 m and 480 m resolutions, 120 m resolution BTL-simulated GPP showed a similar spatial distribution to the reference GPP in low values, while an apparent spatial difference with reference GPP was observed in high values. The GPP estimates were observed to increase in the high values after
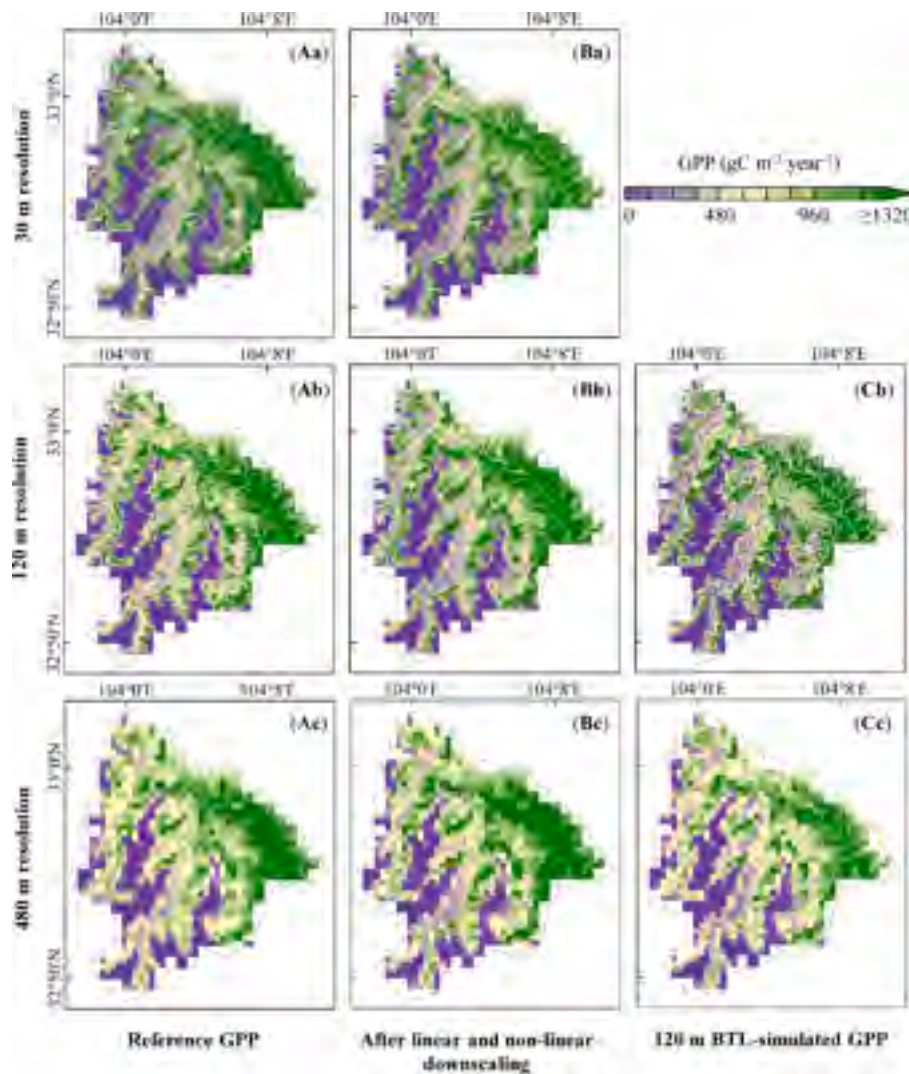
Fig. 5. Spatial distributions of (Aa-Ac) reference GPP, (Ba-Bc) GPP after linear and non-linear downscaling, (Cb-Cc) 120 m resolution BTL-simulated GPP over the CN-WL watershed. The first, second, and third rows are represented at the 30 m, 120 m, and 480 m resolutions, respectively.

applying both the linear and non-linear downscaling processes.

The pixel-based GPP comparisons at the 120 m resolution are shown in Sub-Fig. 6 Ab-Cb. results showed that 120 m resolution BTL-simulated GPP had a moderate relationship with reference GPP, characterized by the d, *RMSE*, and *MAE* values of 0.80, 351, and 256 gC m^{-2} year^{-1}. After applying the linear downscaling process, GPP estimates were found to match better with the reference GPP, with d, *RMSE*, and *MAE* values were improved by 0.08, 106, and 81 gC m^{-2} year^{-1} at the 120 m resolution. GPP estimates after applying both the linear and non-linear downscaling processes were observed to match best with reference GPP at the 120 m resolution, with d, *RMSE*, and *MAE* values were improved by 0.14, 156, and 114 gC m^{-2} year^{-1}, compared to the 120 m resolution BTL-simulated GPP. The GPP comparisons at the 480 m resolution are illustrated in Sub-Fig. 6 Ac-Cc. The d, *RMSE*, and *MAE* values between reference GPP and 120 m resolution BTL-simulated GPP at the 480 m resolution were 0.88, 235, and 178 gC m^{-2} year^{-1}, respectively. Compared to the 120 m resolution BTL-simulated GPP estimates, the d, *RMSE*, and *MAE* values were improved (1) by 0.02, 29, and 23 gC m^{-2} year^{-1} after the linear downscaling and (2) by 0.08, 92, and 72 gC m^{-2} year^{-1} after both the linear and non-linear downscaling at the 480 m resolution.

As listed in Table 2, at the 120 m resolution, the d values of 120 m resolution BTL-simulated GPP in forest, shrub, grass, and crop pixels were 0.77, 0.81, 0.93, and 0.88, respectively. After applying the linear

downscaling process, the d values of GPP estimates in forest, shrub, grass, and crop pixels were increased by 0.07, 0.13, 0.05, and 0.09, respectively. After applying both the linear and non-linear downscaling processes, the d values in forest, shrub, grass, and crop pixels were increased by 0.15, 0.15, 0.05, and 0.09, respectively. At the 120 m resolution, the combination of linear and non-linear downscaling processes increased the d values by 0.08 and 0.02 in forest and shrub pixels, compared to the single linear downscaling.

3.5. Contributions of linear and non-linear downscaling processes across topographic conditions

The d values between reference GPP and 120 m resolution BTL-simulated GPP, GPP after linear downscaling, and GPP after linear and non-linear downscaling in different slope ranges are summarized in Table 3 and Fig. 7. In different slope ranges, d values of 120 m resolution BTL-simulated GPP, GPP after linear downscaling, and GPP after linear and non-linear downscaling ranged from 0.64 to 0.77, 0.70–0.89, and 0.77–0.91, respectively. Results also showed that d between reference GPP and 120 m resolution BTL-simulated GPP increased when the slope varied from 0° to 30°, and presented similar values in the slope ranges of 30°–50°. After applying the linear downscaling process, d was decreased by 0.06–0.12, which usually showed a higher value with an increase in slope. After applying both the linear and non-linear downscaling
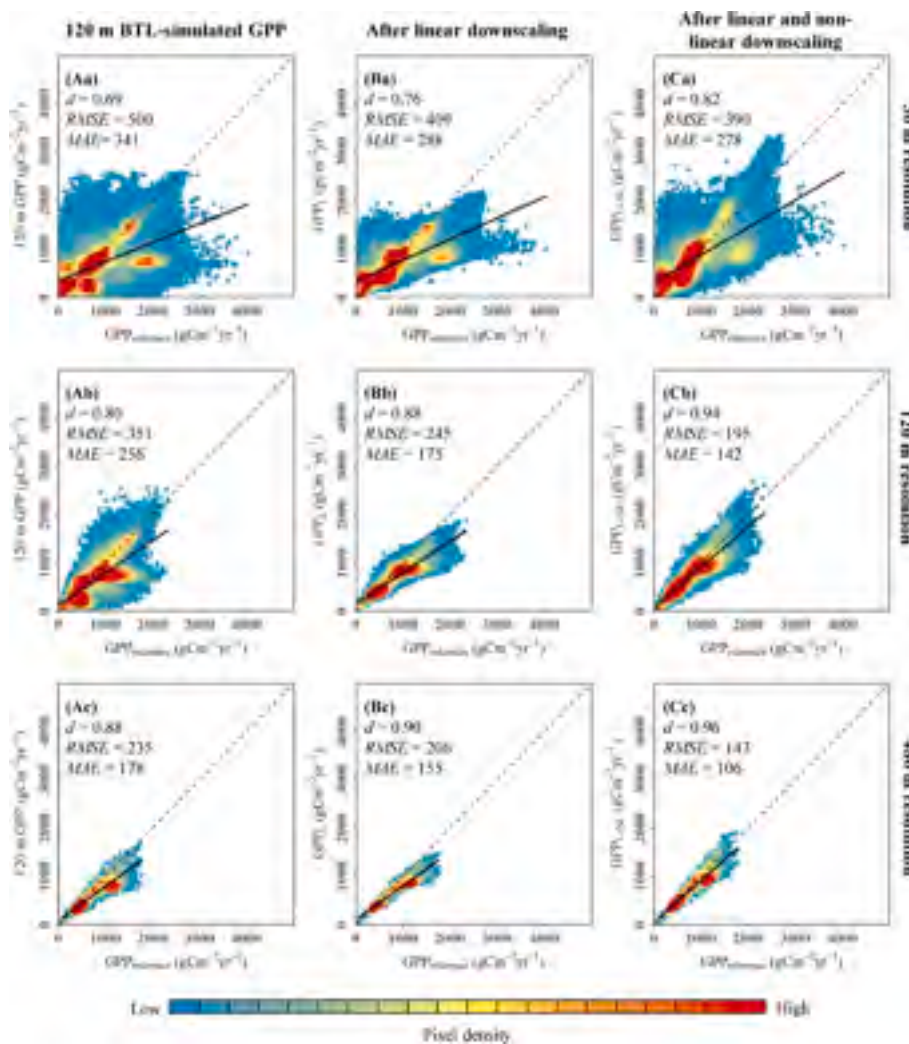
Fig. 6. Relationships between reference GPP and (Aa-Ac) 120 m resolution BTL-simulated GPP, (Ba-Bc) GPP after linear downscaling, and (Ca-Cc) GPP after linear and non-linear downscaling in all pixels over the CN-WL, JP-MBF, US-GLE, and CN-Cha watersheds. The first, second, and third rows are compared at the 30 m, 120 m, and 480 m resolutions, respectively. In the comparison at the 30 m resolution, 120 m resolution BTL-simulated GPP was resampled to 30 m resolution by assuming that all the subpixels have the same value with the corresponding coarse pixel.

Table 2

Agreement index (*d*) values between reference GPP and 120 m resolution BTL-simulated GPP, GPP after linear downscaling, and GPP after linear and non-linear downscaling across vegetation types over the CN-WL, JP-MBF, US-GLE, and CN-Cha watersheds. Agreement index were calculated at the 30 m and 120 m.

GPP type	Vegetation type	Agreement index (d)	
		30 m	120 m
120 m resolution BTL-simulated GPP	Forest	0.65	0.77
	Shrub	0.70	0.81
	Grass	0.82	0.93
	Crop	0.72	0.88
	ALL	0.69	0.80
After linear downscaling	Forest	0.70	0.84
	Shrub	0.83	0.94
	Grass	0.92	0.98
	Crop	0.86	0.97
	ALL	0.76	0.88
After linear and non-linear downscaling	Forest	0.77	0.92
	Shrub	0.87	0.96
	Grass	0.94	0.98
	Crop	0.89	0.97
	ALL	0.82	0.94

Table 3

Agreement index (*d*) between reference GPP and 120 m resolution BTL-simulated GPP, GPP after linear downscaling, and GPP after linear and non-linear downscaling in different slope ranges at the 30 m resolution over the CN-WL, JP-MBF, US-GLE, and CN-Cha watersheds.

Slope (°)	Agreement index (d)[a]		
	120 m resolution BTL-simulated GPP	After linear downscaling	After linear and non-linear downscaling
0–10	0.64	0.71	0.77
10–20	0.64	0.70	0.77
20–30	0.69	0.77	0.83
30–40	0.77	0.87	0.90
40–50	0.77	0.89	0.91

[a] Calculated in each slope range when its total pixel number greater than 500.

processes, *d* was further decreased by 0.02–0.07 (compared to the single linear downscaling process), which showed a lower improvement with an increase in slope.

4. Discussion

4.1. Effectiveness of the proposed scheme in obtaining fine spatial resolution mountain vegetation GPP

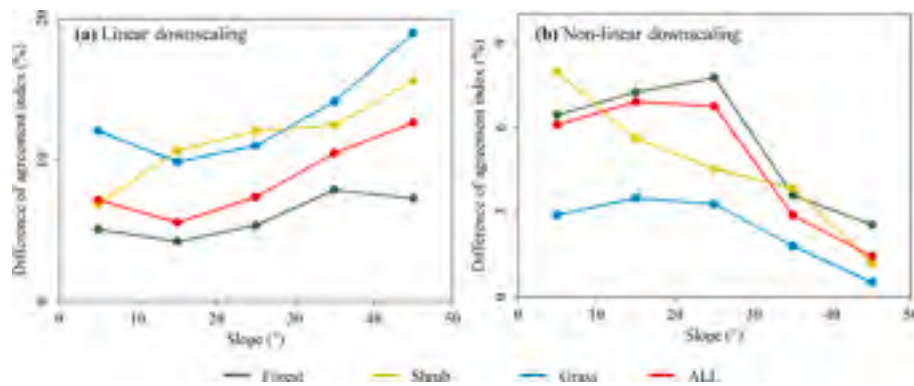Generally, the performances of linear downscaling process at the

Fig. 7. Relationships between slope and agreement index difference of GPP after (a) the linear downscaling compared to 120 m resolution BTL-simulated GPP and (b) non-linear downscaling compared to GPP after linear downscaling at the 30 m resolution over the CN-WL, JP-MBF, US-GLE, and CN-Cha watersheds.

spatial resolutions of 30 m, 120 m, and 480 m were expected because the effect of vegetation heterogeneity, local topographical variations, and long-distance topographical variations on photosynthesis at the watershed scale is still preserved in the 120 m and 480 m resolution GPP estimates. Vegetation heterogeneity has been reported as a determining factor in photosynthesis characteristics associated with vegetation types (He et al., 2019; Jung et al., 2007; Park et al., 2019; Xiao et al., 2011) and the capacity of vegetation photosynthesis related to canopy density and structure (Chen and Black, 1992; Fang et al., 2019). Topographical variations are important in regulating the incoming solar radiation (Yan et al., 2018), movement of the saturated subsurface base flows cycle (Beven et al., 2021; Chen et al., 2005; Wigmosta et al., 1994), and therefore the water availability of vegetation (Ju and Chen, 2005; Ju et al., 2006). The finer spatial resolution that the linear downscaling process is modelled at, the better performance of the linear downscaling process would be.

The linear downscaling process was modelled by assuming that the relationship between coarse resolution estimates and surface heterogeneity is universal at fine spatial resolutions, which is widely adopted in current spatial downscaling algorithms for the estimates of carbon and water fluxes (Ke et al., 2017; Zhao et al., 2018). Although the influence of surface heterogeneity on photosynthesis at the watershed scale is preserved in the 120 m and 480 m resolution GPP estimates, the ignorance of surface heterogeneity within modelling pixels has been reported to cause obvious spatial scaling errors in these coarse resolution estimates (Ahl et al., 2005; Ershadi et al., 2013; Moorcroft et al., 2001). Therefore, GPP estimates after the linear downscaling process might still have biases. For this need, this work innovatively proposed a non-linear downscaling process by the relationships between GPP estimates at the 120 m resolution and the variations of surface heterogeneity from 480 m to 120 m. Compared to the single linear downscaling, the combination of linear and non-linear downscaling processes was observed to achieve a larger improvement of GPP estimates at the spatial resolutions of 30 m, 120 m, and 480 m, because the non-linear downscaling effectively reduced the spatial scaling errors by integrating the variations of vegetation heterogeneity, local topographical variations, and long-distance topographical variations from 120 m to 30 m. For example, Simic et al. (2004) developed a spatial scaling algorithm associated with the spatial information of LAI and LC to correct coarse resolution net primary productivity (NPP) estimates. Based on the effectiveness of endogenous heterogeneity, Chen et al. (2013) further improved the spatial scaling algorithm by adding the local topographical variations (i.e., elevation and slope). Xie et al. (2021a) also moved forward to integrate the algorithm of Chen et al. (2013) with the subpixel information of long-distance topographical variations (i.e., SVF and TWI). In this work, the non-linear downscaling was modelled from 480 m to 120 m resolution, which might lose the capacity to describe the hydrological control of surface topography from 120 m to 30 m. If the non-linear

downscaling was modelled at a finer spatial resolution, the proposed downscaling-based scheme would achieve a better performance.

Overall, results showed that the scheme proposed in this work could effectively recover the topographic features of mountain vegetation GPP at the 30 m resolution and correct GPP spatial scaling errors at the spatial resolutions of 120 m and 480 m. After applying the proposed scheme, a larger improvement was observed in the grass, shrub, and crop pixels than in the forest pixels, because herbaceous vegetation might be more sensitive to surface topography. Previous studies revealed that water availability has an obvious effect in herbaceous vegetation (e.g., grass) (Knapp and Smith, 2001; Liu et al., 2016; Wu et al., 2015). Generally, water storage of the herbaceous vegetation (e.g., grass and shrub) always depends on the quantity of leaf, whereas the woody vegetation can obtain water from deep groundwater.

4.2. Suggestions for obtaining fine spatial resolution mountain vegetation GPP at large scale

Over the last five years, several global vegetation GPP datasets at the 30 m resolution have been generated by executing the GPP models with the RS-based vegetation information at fine spatial resolutions (Huang et al., 2022; Robinson et al., 2018). However, almost all the regional or global GPP datasets are obtained from LUE-based or VI-based approaches. These approaches always estimate GPP without the consideration of surface topography, leading to biases in mountain ecosystems due to the ignored hydrological control of surface topography on the water cycle (Beven et al., 2021; Chen et al., 2005; Wigmosta et al., 1994) and therefore the photosynthesis (Ju and Chen, 2005; Ju et al., 2006). Eco-hydrological models are scientific tools to address the interaction between carbon and water cycles in mountain ecosystems (Govind et al., 2009; Zhang et al., 2018), whereas their regional or global applications at fine spatial resolutions remain difficult due to the complicated model structures. Previous studies have made efforts to modify LUE-based and VI-based models to improve mountain vegetation GPP estimation (Xie and Li, 2020a,b), but the understanding of multiple ecological interactions between surface topography and vegetation photosynthesis in these modified models is not as plentiful as that in the eco-hydrological models.

To develop a general approach that are of interest to carbon modelling in mountain ecosystems, the main purpose of this work is to find an effective way to obtain fine spatial resolution mountain vegetation GPP: (1) the used ecosystem models should have the full ability to describe hydrological control of surface topography on vegetation photosynthesis, (2) the computing resources in the large-scale simulations should be low, and thus it can be easily implemented, and (3) the uncertainties in these fine spatial resolution mountain vegetation GPP estimates should be as low as possible under the above situation of low computing resources. To meet the above requirements, this study firstly

suggested a scheme that runs eco-hydrological models at coarse spatial resolutions and then downscales these coarse estimates by surface heterogeneity, which is a feasible approach for obtaining fine spatial resolution mountain vegetation GPP at large scale.

4.3. Existing limitations in current work

In this work, the random forest algorithm was adopted to model the linear downscaling process and the non-linear downscaling process. It should be noted that the construction of the linear and non-linear downscaling models was restricted to those covered by surface characteristics at the spatial resolutions of 480 m and 120 m. For example, if the coarse resolution pixels used in the construction of downscaling models are all in low slopes, the random forest algorithm would show uncertainties for the 30 m resolution pixels with very high slopes (e.g., >70°). Previous studies also indicated that sufficient pixels under different topographic characteristics are necessary to construct accurate regression models (Hutengs and Vohland, 2016). In this work, the mean values of GPP estimates within the central 1.5 × 1.5 km area at tower sites were compared with EC GPP. A previous study has suggested that the direct use of RS LAI data in ecosystem models would lead to an underestimation in annual GPP (Wang et al., 2019a). GPP directly simulated at 30 m resolution had a lower value than EC GPP in this work, which might be caused by the direct use of current RS LAI. Actually, footprint variation could lead to both over and under estimations of carbon flux due to various wind directions and surface heterogeneity, and more consideration should be given to the flux footprint in the future.

The environmental factors are very necessary in the GPP downscaling process. Three climatic indicators, including precipitation, radiation, and temperature, were obtained from site-based data and then were used in the proposed scheme. As current multiple gridded climatic datasets could provide valuable environmental information at large-scale (Ma et al., 2019a; Ma et al., 2022; Ma et al., 2020), future work should adopt them to obtain mountain vegetation GPP, especially in these areas without site-based climatic measurements.

5. Conclusion

Accurate estimation of mountain vegetation GPP is crucial to understanding the functioning of mountain ecosystems. Eco-hydrological models are scientific tools to simulate the interaction between terrestrial carbon and water cycles in mountain ecosystems, whereas their regional or global applications at fine spatial resolutions remain challenging due to the complicated model structures. To overcome the high computing resources of directly running eco-hydrological models at fine spatial resolutions, a scheme by integrating an eco-hydrological model with a linear downscaling process modelled at the spatial resolution of 120 m and a non-linear downscaling process modelled from 480 m to 120 m resolution, was developed to obtain mountain vegetation GPP at the spatial resolution of 30 m. The GPP estimates obtained by running the BTL model at the 30 m resolution were served as the reference GPP to evaluate the proposed scheme. The main conclusions can be illustrated as:

(1) At the 30 m resolution, results showed that *RMSE* was decreased by 110 gC m^{-2} year^{-1} after the combination of linear and non-linear downscaling processes compared to the 120 m resolution BTL-simulated GPP (*RMSE* = 500 gC m^{-2} year^{-1}), highlighting the effectiveness of the proposed downscaling-based scheme in recovering the topographic variations of mountain vegetation GPP at fine spatial resolutions.

(2) At the 120 m resolution, *RMSE* was observed to decrease by 156 gC m^{-2} year^{-1} after the combination of linear and non-linear downscaling processes compared to the 120 m resolution BTL-simulated GPP (*RMSE* = 351 gC m^{-2} year^{-1}), suggesting that the proposed downscaling-based scheme is feasible in correcting GPP errors at coarse spatial resolutions.

(3) The non-linear downscaling process was observed to effectively improve these GPP estimates after linear downscaling, indicating that the spatial scaling errors in coarse estimates should be considered in the current downscaling algorithm of vegetation productivity.

CRediT authorship contribution statement

Xinyao Xie: Conceptualization, Methodology, Software, Investigation, Visualization, Writing – original draft, Writing – review & editing, Funding acquisition. **Ainong Li:** Supervision, Funding acquisition. **Jie Tian:** Visualization. **Changlin Wu:** Visualization. **Huaan Jin:** Conceptualization, Methodology.

Declaration of Competing Interest

The authors declare that they have no known competing financial interests or personal relationships that could have appeared to influence the work reported in this paper.

Data availability

Data will be made available on request.

References

Ahl, D.E., Gower, S.T., Mackay, D.S., Burrows, S.N., Norman, J.M., Diak, G.R., 2005. The effects of aggregated land cover data on estimating NPP in northern Wisconsin. Remote Sens. Environ. 97, 1–14.

Arain, A.A., Restrepo-Coupe, N., 2005. Net ecosystem production in a temperate pine plantation in southeastern Canada. Agric. For. Meteorol. 128, 223–241.

Aubinet, M., Grelle, A., Ibrom, A., Rannik, U., Moncrieff, J., Foken, T., Kowalski, A.S., Martin, P.H., Berbigier, P., Bernhofer, C., Clement, R., Elbers, J., Granier, A., Grunwald, T., Morgenstern, K., Pilegaard, K., Rebmann, C., Snijders, W., Valentini, R., & Vesala, T. (2000). Estimates of the annual net carbon and water exchange of forests: The EUROFLUX methodology. In A.H. Fitter, & D.G. Raffaelli (Eds.), Advances in Ecological Research, Vol 30 (pp. 113-175).

Baldocchi, D., Falge, E., Gu, L.H., Olson, R., Hollinger, D., Running, S., Anthoni, P., Bernhofer, C., Davis, K., Evans, R., Fuentes, J., Goldstein, A., Katul, G., Law, B., Lee, X.H., Malhi, Y., Meyers, T., Munger, W., Oechel, W., Pilegaard, K., Schmid, H.P., Valentini, R., Verma, S., Vesala, T., Wilson, K., Wofsy, S., 2001. FLUXNET: A new tool to study the temporal and spatial variability of ecosystem-scale carbon dioxide, water vapor, and energy flux densities. Bull. Am. Meteorol. Soc. 82, 2415–2434.

Band, L.E., Patterson, P., Nemani, R., Running, S.W., 1993. Forest ecosystem processes at the watershed scale - incorporating hillslope hydrology. Agric. For. Meteorol. 63, 93–126.

Bandyopadhyay, J., Rodda, J.C., Kattelman, R., Kundzwicz, Z.W., Ives, J.D., 1997. Highland waters - a resource of global significance. Mountains of the World.

Beringer, J., Hutley, L.B., McHugh, I., Arndt, S.K., Campbell, D., Cleugh, H.A., Cleverly, J., de Dios, V.R., Eamus, D., Evans, B., Ewenz, C., Grace, P., Griebel, A., Haverd, V., Hinko-Najera, N., Huete, A., Isaac, P., Kanniah, K., Leuning, R., Liddell, M.J., Macfarlane, C., Meyer, W., Moore, C., Pendall, E., Phillips, A., Phillips, R.L., Prober, S.M., Restrepo-Coupe, N., Rutledge, S., Schroder, I., Silberstein, R., Southall, P., Yee, M.S., Tapper, N.J., van Gorsel, E., Vote, C., Walker, J., Wardlaw, T., 2016. An introduction to the Australian and New Zealand flux tower network - OzFlux. Biogeosciences 13, 5895–5916.

Beven, K.J., Kirkby, M.J., Freer, J.E., Lamb, R., 2021. A history of TOPMODEL. Hydrol. Earth Syst. Sci. 25, 527–549.

Bhattacharyya, P., Neogi, S., Roy, K.S., Rao, K.S., 2013. Gross primary production, ecosystem respiration and net ecosystem exchange in Asian rice paddy: an eddy covariance-based approach. Curr. Sci. 104, 67–75.

Breiman, L., Breiman, L., Cutler, R.A.J.J.O.C.M., 2001. Random Forests. Mach. Learn. 2, 199–228.

Chen, J.M., Black, T.A., 1992. Defining leaf-area index for non-flat leaves. Plant Cell Environ. 15, 421–429.

Chen, J.M., Liu, J., Cihlar, J., Goulden, M.L., 1999. Daily canopy photosynthesis model through temporal and spatial scaling for remote sensing applications. Ecol. Model. 124, 99–119.

Chen, J.M., Chen, X.Y., Ju, W.M., Geng, X.Y., 2005. Distributed hydrological model for mapping evapotranspiration using remote sensing inputs. J. Hydrol. 305, 15–39.

Chen, J.M., Mo, G., Pisek, J., Liu, J., Deng, F., Ishizawa, M., Chan, D., 2012. Effects of foliage clumping on the estimation of global terrestrial gross primary productivity. Global Biogeochem. Cycles 26, 18.

Chen, J.M., Chen, X., Ju, W., 2013. Effects of vegetation heterogeneity and surface topography on spatial scaling of net primary productivity. Biogeosciences 10, 4879–4896.

Ershadi, A., McCabe, M.F., Evans, J.P., Walker, J.P., 2013. Effects of spatial aggregation on the multi-scale estimation of evapotranspiration. Remote Sens. Environ. 131, 51–62.

Fang, H., Baret, F., Plummer, S., Schaepman-Strub, G., 2019. An Overview of Global Leaf Area Index (LAI): Methods, Products, Validation, and Applications. Rev. Geophys. 57, 739–799.

Farquhar, G.D., Caemmerer, S.V., Berry, J.A., 1980. A biochemical-model of photosynthetic CO2 assimilation in leaves of C-3 Species. Planta 149, 78–90.

Foley, J.A., Prentice, I.C., Ramankutty, N., Levis, S., Pollard, D., Sitch, S., Haxeltine, A., 1996. An integrated biosphere model of land surface processes, terrestrial carbon balance, and vegetation dynamics. Global Biogeochem. Cycles 10, 603–628.

Gong, P., Wang, J., Yu, L., Zhao, Y.C., Zhao, Y.Y., Liang, L., Niu, Z.G., Huang, X.M., Fu, H. H., Liu, S., Li, C.C., Li, X.Y., Fu, W., Liu, C.X., Xu, Y., Wang, X.Y., Cheng, Q., Hu, L.Y., Yao, W.B., Zhang, H., Zhu, P., Zhao, Z.Y., Zhang, H.Y., Zheng, Y.M., Ji, L.Y., Zhang, Y.W., Chen, H., Yan, A., Guo, J.H., Yu, L., Wang, L., Liu, X.J., Shi, T.T., Zhu, M.H., Chen, Y.L., Yang, G.W., Tang, P., Xu, B., Giri, C., Clinton, N., Zhu, Z.L., Chen, J., Chen, J., 2013. Finer resolution observation and monitoring of global land cover: first mapping results with Landsat TM and ETM+ data. Int. J. Remote Sens. 34, 2607–2654.

Govind, A., Chen, J.M., Margolis, H., Ju, W., Sonnentag, O., Giasson, M.-A., 2009. A spatially explicit hydro-ecological modeling framework (BEPS-TerrainLab V2.0): Model description and test in a boreal ecosystem in Eastern North America. J. Hydrol. 367, 200–216.

Guan, X., Chen, J.M., Shen, H., Xie, X., 2021. A modified two-leaf light use efficiency model for improving the simulation of GPP using a radiation scalar. Agric. For. Meteorol. 307, 108546.

Guan, D.-X., Wu, J.-B., Zhao, X.-S., Han, S.-J., Yu, G.-R., Sun, X.-M., Jin, C.-J., 2006. CO2 fluxes over an old, temperate mixed forest in northeastern China. Agric. For. Meteorol. 137, 138–149.

Harris, P.P., Huntingford, C., Cox, P.M., Gash, J.H.C., Malhi, Y., 2004. Effect of soil moisture on canopy conductance of Amazonian rainforest. Agric. For. Meteorol. 122, 215–227.

He, L.M., Chen, J.M., Liu, J.N., Zheng, T., Wang, R., Joiner, J., Chou, S.R., Cheng, B., Liu, Y., Liu, R.G., Rogers, C., 2019. Diverse photosynthetic capacity of global ecosystems mapped by satellite chlorophyll fluorescence measurements. Remote Sens. Environ. 232, 10.

He, M., Ju, W., Zhou, Y., Chen, J., He, H., Wang, S., Wang, H., Guan, D., Yan, J., Li, Y., Hao, Y., Zhao, F., 2013. Development of a two-leaf light use efficiency model for improving the calculation of terrestrial gross primary productivity. Agric. For. Meteorol. 173, 28–39.

Hengl, T., de Jesus, J.M., Heuvelink, G.B.M., Gonzalez, M.R., Kilibarda, M., Blagotic, A., Shangguan, W., Wright, M.N., Geng, X., Bauer-Marschallinger, B., Guevara, M.A., Vargas, R., MacMillan, R.A., Batjes, N.H., Leenaars, J.G.B., Ribeiro, E., Wheeler, I., Mantel, S., & Kempen, B. (2017). SoilGrids250m: Global gridded soil information based on machine learning. *Plos One, 12.*

Henry, M., Picard, N., Trotta, C., Manlay, R.J., Valentini, R., Bernoux, M., Saint-Andre, L., 2011. Estimating Tree Biomass of Sub-Saharan African Forests: a Review of Available Allometric Equations. Silva Fennica 45, 477–569.

Hilton, R.G., West, A.J., 2020. Mountains, erosion and the carbon cycle. Nat. Rev. Earth Environ. 1, 284–299.

Houborg, R., McCabe, M.F., 2018. A hybrid training approach for leaf area index estimation via Cubist and random forests machine-learning. ISPRS J. Photogramm. Remote Sens. 135, 173–188.

Huang, X., Zheng, Y., Zhang, H., Lin, S., Liang, S., Li, X., Ma, M., Yuan, W., 2022. High spatial resolution vegetation gross primary production product: Algorithm and validation. Science of Remote Sensing 100049.

Hutengs, C., Vohland, M., 2016. Downscaling land surface temperatures at regional scales with random forest regression. Remote Sens. Environ. 178, 127–141.

Jarvis, P.G., 1976. Interpretation of variations in leaf water potential and stomatal conductance found in canopies in field. Philos. Trans. R. Soc. Lond. Ser. B-Biol. Sci. 273, 593–610.

Ju, W.M., Chen, J.M., 2005. Distribution of soil carbon stocks in Canada's forests and wetlands simulated based on drainage class, topography and remotely sensed vegetation parameters. Hydrol. Process. 19, 77–94.

Ju, W.M., Chen, J.M., Black, T.A., Barr, A.G., Mccaughey, H., Roulet, N.T., 2006. Hydrological effects on carbon cycles of Canada's forests and wetlands. Tellus Series B-Chem. Phys. Meteorol. 58, 16–30.

Jung, M., 2019. The FLUXCOM ensemble of global land-atmosphere energy fluxes. Scientific Data.

Jung, M., Vetter, M., Herold, M., Churkina, G., Reichstein, M., Zaehle, S., Ciais, P., Viovy, N., Bondeau, A., Chen, Y., Trusilova, K., Feser, F., Heimann, M., 2007. Uncertainties of modeling gross primary productivity over Europe: A systematic study on the effects of using different drivers and terrestrial biosphere models. Global Biogeochem. Cycles 21.

Kapos, V., Rhind, J., Edwards, M., Price, M., Ravilious, C., & Butt, N. (2000). Developing a map of the world's mountain forests., Forests in sustainable mountain development: a state of knowledge report for 2000. *Task Force For. Sustain. Mt. Dev.,* 4-19.

Ke, Y.H., Im, J., Park, S., Gong, H.L., 2017. Spatiotemporal downscaling approaches for monitoring 8-day 30 m actual evapotranspiration. ISPRS J. Photogramm. Remote Sens. 126, 79–93.

Kljun, N., Calanca, P., Rotach, M.W., Schmid, H.P., 2015. A simple two-dimensional parameterisation for Flux Footprint Prediction (FFP). Geosci. Model Dev. 8, 3695–3713.

Knapp, A.K., Smith, M.D., 2001. Variation among biomes in temporal dynamics of aboveground primary production. Science 291, 481–484.

Liang, S., Cheng, J., Jia, K., Jiang, B., Liu, Q., Xiao, Z., Yao, Y., Yuan, W., Zhang, X., Zhao, X., Zhou, J., 2021. The Global Land Surface Satellite (GLASS) Product Suite. Bull. Am. Meteorol. Soc. 102, E323–E337.

Liu, Y., Xiao, J., Ju, W., Zhu, G., Wu, X., Fan, W., Li, D., Zhou, Y., 2018. Satellite-derived LAI products exhibit large discrepancies and can lead to substantial uncertainty in simulated carbon and water fluxes. Remote Sens. Environ. 206, 174–188.

Liu, S., Zhuang, Q., He, Y., Noormets, A., Chen, J., Gu, L., 2016. Evaluating atmospheric CO2 effects on gross primary productivity and net ecosystem exchanges of terrestrial ecosystems in the conterminous United States using the AmeriFlux data and an artificial neural network approach. Agric. For. Meteorol. 220, 38–49.

Ma, Z., Xu, J., Ma, Y., Zhu, S., He, K., Zhang, S., Ma, W., & Xu, X. (2022). AERA5-Asia: A long-term Asian precipitation dataset (0.1°, 1 hourly, 1951–2015, Asia) anchoring the ERA5-Land under the total volume control by APHRODITE. *Bulletin of the American Meteorological Society, 103,* 1.

Ma, Z., Shi, Z., Zhou, Y., Xu, J., Yu, W., Yang, Y., 2017a. A spatial data mining algorithm for downscaling TMPA 3B43 V7 data over the Qinghai-Tibet Plateau with the effects of systematic anomalies removed. Remote Sens. Environ. 200.

Ma, Z., Zhou, Y., Hu, B., Liang, Z., Shi, Z., 2017b. Downscaling annual precipitation with TMPA and land surface characteristics in China: satellite-based precipitation estimates with high spatial resolution. Int. J. Climatol. 37.

Ma, Z., Tan, X., Yang, Y., Xi, C., Kan, G., Ji, X., Lu, H., Long, J., Cui, Y., Hong, Y., 2018. The First Comparisons of IMERG and the Downscaled Results Based on IMERG in Hydrological Utility over the Ganjiang River Basin. Water 10.

Ma, Z., Ghent, D., Han, X., Li, H., Tan, X., He, K., Huang, Q., Peng, J., 2019a. Long-Term Precipitation Estimates Generated by a Downscaling-Calibration Procedure. In: Over the Tibetan Plateau from 1983 to 2015. *Earth and Space Science,* p. 6.

Ma, Z., Xu, J., He, K., Han, X., Ji, Q., Tsechun, W., Xiong, W., Hong, Y., 2019b. An updated moving window algorithm for hourly-scale satellite precipitation downscaling: A case study in the Southeast Coast of China. J. Hydrol. 581, 124378.

Ma, Z., Xu, J., Zhu, S., Yang, J., Tang, G., Yang, Y., Shi, Z., Hong, Y., 2020. AIMERG: a new Asian precipitation dataset (0.1°/half-hourly, 2000–2015) by calibrating the GPM-era IMERG at a daily scale using APHRODITE. Earth Syst. Sci. Data 12, 1525–1544.

Matsumoto, K., Ohta, T., Nakai, T., Kuwada, T., Daikoku, K.i., Iida, S.i., Yabuki, H., Kononov, A.V., van der Molen, M.K., Kodama, Y., Maximov, T.C., Dolman, A.J., Hattori, S. (2008). Energy consumption and evapotranspiration at several boreal and temperate forests in the Far East. Agric. Forest Meteorol., 148, 1978-1999.

Mizoguchi, Y., Miyata, A., Ohtani, Y., Hirata, R., Yuta, S., 2009. A review of tower flux observation sites in Asia. J. For. Res. 14, 1–9.

Moorcroft, P.R., Hurtt, G.C., Pacala, S.W., 2001. A method for scaling vegetation dynamics: The ecosystem demography model (ED). Ecol. Monogr. 71, 557–585.

Novick, K.A., Biederman, J.A., Desai, A.R., Litvak, M.E., Moore, D.J.P., Scott, R.L., Torn, M.S., 2018. The AmeriFlux network: A coalition of the willing. Agric. For. Meteorol. 249, 444–456.

Park, H., Im, J., Kim, M., 2019. Improvement of satellite-based estimation of gross primary production through optimization of meteorological parameters and high resolution land cover information at regional scale over East Asia. Agric. For. Meteorol. 271, 180–192.

Robinson, N.P., Allred, B.W., Smith, W.K., Jones, M.O., Moreno, A., Erickson, T.A., Naugle, D.E., Running, S.W., 2018. Terrestrial primary production for the conterminous United States derived from Landsat 30 m and MODIS 250 m. Remote Sens. Ecol. Conserv. 4, 264–280.

Running, S., Mu, Q., Zhao, M., 2015. MOD17A2H MODIS/Terra Gross Primary Productivity 8-Day L4 Global 500m SIN Grid V006. NASA EOSDIS Land Processes. DAAC.https://doi.org/10.5067/MODIS/MOD17A2H.006.

Running, S.W., Nemani, R.R., Heinsch, F.A., Zhao, M.S., Reeves, M., Hashimoto, H., 2004. A continuous satellite-derived measure of global terrestrial primary production. Bioscience 54, 547–560.

Simic, A., Chen, J.M., Liu, J., Csillag, F., 2004. Spatial scaling of net primary productivity using subpixel information. Remote Sens. Environ. 93, 246–258.

Sims, D.A., Rahman, A.F., Cordova, V.D., El-Masri, B.Z., Baldocchi, D.D., Bolstad, P.V., Flanagan, L.B., Goldstein, A.H., Hollinger, D.Y., Misson, L., Monson, R.K., Oechel, W. C., Schmid, H.P., Wofsy, S.C., Xu, L., 2008. A new model of gross primary productivity for North American ecosystems based solely on the enhanced

vegetation index and land surface temperature from MODIS. Remote Sens. Environ. 112, 1633–1646.

Sorensen, R., Zinko, U., Seibert, J., 2006. On the calculation of the topographic wetness index: evaluation of different methods based on field observations. Hydrol. Earth Syst. Sci. 10, 101–112.

Steinbauer, M.J., Grytnes, J.-A., Jurasinski, G., Kulonen, A., Lenoir, J., Pauli, H., Rixen, C., Winkler, M., Bardy-Durchhalter, M., Barni, E., Bjorkman, A.D., Breiner, F.T., Burg, S., Czortek, P., Dawes, M.A., Delimat, A., Dullinger, S., Erschbamer, B., Felde, V.A., Fernandez-Arberas, O., Fossheim, K.F., Gomez-Garcia, D., Georges, D., Grindrud, E.T., Haider, S., Haugum, S.V., Henriksen, H., Herreros, M.J., Jaroszewicz, B., Jaroszynska, F., Kanka, R., Kapfer, J., Klanderud, K., Kuhn, I., Lamprecht, A., Matteodo, M., di Cella, U.M., Normand, S., Odland, A., Olsen, S.L., Palacio, S., Petey, M., Piscova, V., Sedlakova, B., Steinbauer, K., Stockli, V., Svenning, J.-C., Teppa, G., Theurillat, J.-P., Vittoz, P., Woodin, S.J., Zimmermann, N.E., Wipf, S., 2018. Accelerated increase in plant species richness on mountain summits is linked to warming. Nature, *556*, 231-+.

Tagesson, T., Tian, F., Schurgers, G., Horion, S., Scholes, R., Ahlstrom, A., Ardo, J., Moreno, A., Madani, N., Olin, S., Fensholt, R., 2021. A physiology-based Earth observation model indicates stagnation in the global gross primary production during recent decades. Glob. Chang. Biol. 27, 836–854.

Tan, Z.-H., Zhao, J.-F., Wang, G.-Z., Chen, M.-P., Yang, L.-Y., He, C.-S., Restrepo-Coupe, N., Peng, S.-S., Liu, X.-Y., da Rocha, H.R., Kosugi, Y., Hirano, T., Salesk, S.R., Goulden, M.L., Zeng, J., Ding, F.-J., Gao, F., Song, L., 2019. Surface conductance for evapotranspiration of tropical forests: Calculations, variations, and controls. Agric. For. Meteorol. 275, 317–328.

Tramontana, G., Jung, M., Schwalm, C.R., Ichii, K., Camps-Valls, G., Raduly, B., Reichstein, M., Arain, M.A., Cescatti, A., Kiely, G., Merbold, L., Serrano-Ortiz, P., Sickert, S., Wolf, S., Papale, D., 2016. Predicting carbon dioxide and energy fluxes across global FLUXNET sites with regression algorithms. Biogeosciences 13, 4291–4313.

van Zyl, J.J., 2001. The Shuttle Radar Topography Mission (SRTM): A breakthrough in remote sensing of topography. Acta Astronaut. 48, 559–565.

Viviroli, D., Archer, D.R., Buytaert, W., Fowler, H.J., Greenwood, G.B., Hamlet, A.F., Huang, Y., Koboltschnig, G., Litaor, M.I., Lopez-Moreno, J.I., Lorentz, S., Schadler, B., Schreier, H., Schwaiger, K., Vuille, M., Woods, R., 2011. Climate change and mountain water resources: overview and recommendations for research, management and policy. Hydrol. Earth Syst. Sci. 15, 471–504.

Wang, R., Chen, J.M., Luo, X.Z., Black, A., Arain, A., 2019a. Seasonality of leaf area index and photosynthetic capacity for better estimation of carbon and water fluxes in evergreen conifer forests. Agric. For. Meteorol. 279, 15.

Wang, S., Garcia, M., Bauer-Gottwein, P., Jakobsen, J., Zarco-Tejada, P.J., Bandini, F., Paz, V.S., Ibrom, A., 2019b. High spatial resolution monitoring land surface energy, water and CO2 fluxes from an Unmanned Aerial System. Remote Sens. Environ. 229, 14–31.

Wigmosta, M.S., Vail, L.W., Lettenmaier, D.P., 1994. A distributed hydrology-vegetation model for complex terrain. Water Resour. Res. 30, 1665–1679.

Wu, C.Y., Chen, J.M., Huang, N., 2011. Predicting gross primary production from the enhanced vegetation index and photosynthetically active radiation: Evaluation and calibration. Remote Sens. Environ. 115, 3424–3435.

Wu, D., Zhao, X., Liang, S., Zhou, T., Huang, K., Tang, B., Zhao, W., 2015. Time-lag effects of global vegetation responses to climate change. Glob. Chang. Biol. 21, 3520–3531.

Wutzler, T., Lucas-Moffat, A., Migliavacca, M., Knauer, J., Sickel, K., Sigut, L., Menzer, O., Reichstein, M., 2018. Basic and extensible post-processing of eddy covariance flux data with REddyProc. Biogeosciences 15, 5015–5030.

Xiao, J.F., Chevallier, F., Gomez, C., Guanter, L., Hicke, J.A., Huete, A.R., Ichii, K., Ni, W. J., Pang, Y., Rahman, A.F., Sun, G.Q., Yuan, W.P., Zhang, L., Zhang, X.Y., 2019.

Remote sensing of the terrestrial carbon cycle: A review of advances over 50 years. Remote Sens. Environ. 233, 37.

Xiao, J., Davis, K.J., Urban, N.M., Keller, K., Saliendra, N.Z., 2011. Upscaling carbon fluxes from towers to the regional scale: Influence of parameter variability and land cover representation on regional flux estimates. J. Geophys. Res.-Biogeosci. 116.

Xiao, X.M., Hollinger, D., Aber, J., Goltz, M., Davidson, E.A., Zhang, Q.Y., Moore, B., 2004. Satellite-based modeling of gross primary production in an evergreen needleleaf forest. Remote Sens. Environ. 89, 519–534.

Xie, X., Li, A., 2020a. An Adjusted Two-Leaf Light Use Efficiency Model for Improving GPP Simulations Over Mountainous Areas. Journal of Geophysical Research: Atmospheres, 125, e2019JD031702.

Xie, X., Chen, J.M., Gong, P., & Li, A. (2021a). Spatial scaling of gross primary productivity over sixteen mountainous watersheds using vegetation heterogeneity and surface topography. J. Geophys. Res.: Biogeosci., 126, e2020JG005848.

Xie, X., Li, A., Chen, J.M., Guan, X., Leng, J., 2022. Quantifying Scaling Effect on Gross Primary Productivity Estimation in the Upscaling Process of Surface Heterogeneity. J. Geophy. Res.: Biogeosci., 127, e2021JG006775.

Xie, X., Li, A., 2020b. Development of a topographic-corrected temperature and greenness model (TG) for improving GPP estimation over mountainous areas. Agric. For. Meteorol. 295, 108193.

Xie, X., Li, A., Jin, H., Bian, J., Zhang, Z., Nan, X., 2021b. Comparing three remotely sensed approaches for simulating gross primary productivity over Mountainous Watersheds: A Case Study in the Wanglang National Nature Reserve, China. *Remote Sensing* 13, 3567.

Xu, C., McDowell, N.G., Fisher, R.A., Wei, L., Sevanto, S., Christoffersen, B.O., Weng, E., Middleton, R.S., 2019. Increasing impacts of extreme droughts on vegetation productivity under climate change. Nat. Clim. Chang. 9, 948–953.

Yan, G., Tong, Y., Yan, K., Mu, X., Chu, Q., Zhou, Y., Liu, Y., Qi, J., Lio, L., Zeng, Y., Zhou, H., Xie, D., Zhang, W., 2018. Temporal extrapolation of daily downward shortwave radiation over cloud-free rugged terrains. Part 1: analysis of topographic effects. IEEE Trans. Geosci. Remote Sens. 56, 6375–6394.

Yang, X., Xu, M., 2003. Biodiversity conservation in Changbai Mountain Biosphere Reserve, northeastern China: Status, problem, and strategy. Biodivers. Conserv. 12, 883–903.

Yuan, W., Liu, S., Yu, G., Bonnefond, J.-M., Chen, J., Davis, K., Desai, A.R., Goldstein, A. H., Gianelle, D., Rossi, F., Suyker, A.E., Verma, S.B., 2010. Global estimates of evapotranspiration and gross primary production based on MODIS and global meteorology data. Remote Sens. Environ. 114, 1416–1431.

Yuan, W., Zheng, Y., Piao, S., Ciais, P., Lombardozzi, D., Wang, Y., Ryu, Y., Chen, G., Dong, W., Hu, Z., Jain, A.K., Jiang, C., Kato, E., Li, S., Lienert, S., Liu, S., Nabel, J.E. M.S., Qin, Z., Quine, T., Sitch, S., Smith, W.K., Wang, F., Wu, C., Xiao, Z., Yang, S., 2019. Increased atmospheric vapor pressure deficit reduces global vegetation growth. Sci. Adv. 5.

Zaksek, K., Ostir, K., Kokalj, Z., 2011. Sky-view factor as a relief visualization technique. Remote Sens. (Basel) 3, 398–415.

Zhang, W., Li, Y., Zhu, B., Zheng, X., Liu, C., Tang, J., Su, F., Zhang, C., Ju, X., Deng, J., 2018. A process-oriented hydro-biogeochemical model enabling simulation of gaseous carbon and nitrogen emissions and hydrologic nitrogen losses from a subtropical catchment. Sci. Total Environ. 616, 305–317.

Zhang, Y., Xiao, X., Wu, X., Zhou, S., Zhang, G., Qin, Y., Dong, J., 2017. Data Descriptor: A global moderate resolution dataset of gross primary production of vegetation for 2000–2016. Scientific Data, p. 4.

Zhao, W., Sanchez, N., Lu, H., Li, A., 2018. A spatial downscaling approach for the SMAP passive surface soil moisture product using random forest regression. J. Hydrol. 563, 1009–1024.

Zhao, W., Duan, S.-B., Li, A., Yin, G., 2019. A practical method for reducing terrain effect on land surface temperature using random forest regression. Remote Sens. Environ. 221, 635–649.